CORROSION SCIENCE AND TECHNOLOGY, Vol.3, No.5(2004), pp.198~208

In-situ Raman Spectroscopic Study of Nickel-base Alloys in Nuclear Power Plants and Its Implications to SCC

Ji Hyun Kim*, Chi Bum Bahn, and Il Soon Hwang

Department of Nuclear Engineering, Seoul National University, Seoul, Republic of Korea
56-1 Shinlim-dong, Gwanak-gu, Seoul 151-742
**Department of Nuclear Engineering, Massachusetts Institute of Technology, Cambridge, MA 02139, USA*

Although there has been no general agreement on the mechanism of primary water stress corrosion cracking (PWSCC) as one of major degradation modes of Ni-base alloys in pressurized water reactors (PWR's), common postulation derived from previous studies is that the damage to the alloy substrate can be related to mass transport characteristics and/or repair properties of overlaid oxide film. Recently, it was shown that the oxide film structure and PWSCC initiation time as well as crack growth rate were systematically varied as a function of dissolved hydrogen concentration in high temperature water, supporting the postulation. In order to understand how the oxide film composition can vary with water chemistry, this study was conducted to characterize oxide films on Alloy 600 by an in-situ Raman spectroscopy. Based on both experimental and thermodynamic prediction results, Ni/NiO thermodynamic equilibrium condition was defined as a function of electrochemical potential and temperature. The results agree well with Attanasio et al.'s data by contact electrical resistance measurements. The anomalously high PWSCC growth rate consistently observed in the vicinity of Ni/NiO equilibrium is then attributed to weak thermodynamic stability of NiO. Redox-induced phase transition between Ni metal and NiO may undermine the integrity of NiO and enhance presumably the percolation of oxidizing environment through the oxide film, especially along grain boundaries. The redox-induced grain boundary oxide degradation mechanism has been postulated and will be tested by using the in-situ Raman facility.

Keywords *: primary water stress corrosion cracking (PWSCC), Alloy 600, in-situ Raman spectroscopy, oxide film, Ni/NiO thermodynamic equilibrium, dissolved hydrogen concentration, phase transition*

1. Introduction

Primary water stress corrosion cracking (PWSCC) is one of major degradation modes that have been observed to occur predominantly along grain boundaries in a Ni-base Alloy 600 for steam generator (SG) tubes and penetration nozzles in the primary circuit of PWR's. Such an intergranular stress corrosion cracking (IGSCC) has been observed under specific combinations of materials and environmental conditions.[1] The PWSCC of Alloy 600 components is directly related with safety concerns as the root cause of potential rupture of SG tubes or nozzle ejection despite the fact that they have relatively large safety margins. With increasing number of plants operating beyond their design lives, rapidly growing numbers of PWSCC are observed in Ni-base components that are critical to the plant reliability.

The PWSCC phenomenon of Alloy 600 has been extensively studied primarily to establish empirical models for predicting the crack initiation time and crack growth rates for field components.[2)-7)] In order to formulate more fundamental solutions, it is necessary to understand PWSCC mechanism. Mechanistic models proposed to date are based on slip-dissolution/oxidation,[2)] corrosion-enhanced plasticity,[3)] internal oxidation[4),5)] and creep.[6),7)] Even though there is no satisfactory agreement as to the mechanism of PWSCC, one common postulation is that the damage to the alloy substrate can be related to mass transport characteristics, rupture and/or repair properties of overlaid oxide film.

Earlier studies have shown that dissolved hydrogen concentration in high temperature water affects the PWSCC susceptibility of nickel base alloys.[3),8)-11)] These results have highlighted that the crack growth rate at a given stress intensity factor and temperature displays a bell-shape peak in the vicinity of dissolved hydrogen concentration that corresponds to thermodynamic equilibrium between nickel metal (Ni) and nickel oxide (NiO),

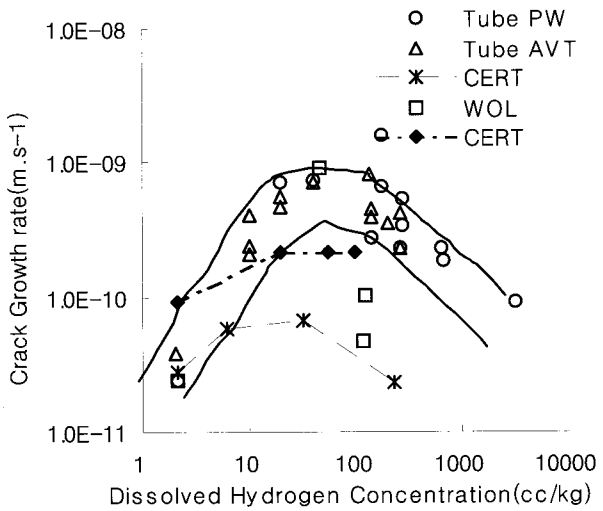

Fig. 1. Influence of hydrogen concentration on the crack growth rate of PWSCC in Alloy 600 at 360℃.[10),11)]

as shown in Fig. 1.[10), 11)] More recently, it was also shown that the oxide film structure, PWSCC initiation time and crack growth rate were systematically varied as a function of hydrogen partial pressure in high temperature water.[10)-12)] These observations are believed to constitute strong evidences that the nature of oxide film on the surface of Alloy 600 plays a key role in the process of PWSCC.

To date, oxide film characterizations for Alloy 600 exposed to PWR water have been made only by ex-situ methods.[10),12),32)] Since domains of oxide stability changes significantly with temperature and water chemistry, as evidenced in the case of Ni/NiO, an in-situ examination is highly desired. The present study is aimed at a direct characterization of the chemistry and structure of oxide film by in-situ Raman spectroscopy under PWR primary water conditions in order to verify earlier results and obtain basic information conducive to mechanistic understanding. In-situ Raman spectroscopy can be conducted by analyzing oxide film properties using reflected laser beam through a hermetically sealed window in various conditions exhibiting different PWSCC susceptibilities The Raman system developed in this study is capable of examining the effect of temperature, dissolved hydrogen concentration, strain and impurity concentration on oxide film behavior at temperature of up to 350℃ and pressure of up to 18 MPa. Observed results were compared with thermodynamic calculations for the thermodynamically stable oxide phases so that meaningful conclusions can be drawn.

Table 1. Chemical Composition of Alloy 600 Used in This Study (wt.%).

Element	Composition
C	0.06
Mn	0.26
Fe	8.31
S	0.001
Si	0.3
Cu	0.12
Ni	75.12
Cr	15.25
Al	0.16
Ti	0.36
Nb	0.04
P	0.09
B	0.02
N	0.01

2. Experimental

2.1 Materials for Raman spectroscopy

The Alloy 600 used in this work for analysis of the oxide films have been produced by Sumitomo Metals, Inc. following typical specification of a reactor pressure vessel (RPV) head penetration nozzles in PWRs, for the EAC-J round robin test under the auspice of the International Cooperative Group on Environmentally Assisted Cracking (ICG-EAC). Chemical composition of Alloy 600 used in this study is given in Table 1. The material was supplied in the condition of solution-annealed at 1050℃ for 2 hours followed by water-cooling. Its microstructure showed partially solutionized carbides with an average grain size of about 50 (m. Alloy 600 specimens for the in-situ Raman spectroscopy was machined by electro-discharge machining (EDM) in the form of a disk with 7 mm diameter and 1 mm thickness. All the machined specimens were mechanically polished down to 1μm Al_2O_3 powder, then rinsed with ethanol, and finally with deionized water prior to installation in the high pressure cell.

To obtain reference Raman spectra, the commercial high purity powders of NiO (99.998%), $NiFe_2O_4$ (99%), Cr_2O_3 (99.998%), and $NiCr_2O_4$ (90%) were loaded on the developed Raman system and measurements were made in room temperature and air condition. Average particle size of high purity powder was 44 μm for NiO, 200 μm for $NiFe_2O_4$, 800 μm for Cr_2O_3, and 150 μm for $NiCr_2O_4$. Powder color was dark green for NiO, brown for $NiFe_2O_4$, and green for Cr_2O_3 and $NiCr_2O_4$. Powder samples were mixed with deionized water, placed in the recess of sample holder, and finally dried to obtain aggregate deposition on the sample holder.

2.2 Test conditions

For the surface oxide formation, the Alloy 600 specimens were exposed to simulated PWR primary water environments inside the high-pressure cell. The cell for the in-situ observation at high temperature and pressure condition was constructed with a custom-designed 1 liter-capacity autoclave. The cell was made of Alloy 690 and a water-mixing tank was made of titanium. The head of a water-charging pump was made of titanium and balls of check valves were made of sapphire. All other components exposed to high temperature water including compression fittings and tubing were made of Alloy 600. The nominal flow rate to the cell was maintained at 4 liters per hour during experiments.

The cylindrical cell was machined with two penetrations in the sidewall to accommodate optical windows for the Raman spectroscopy. The initial window assembly, composed of 4.5 mm thick sapphire with gaskets to seal high-pressure water, was designed after Hurst et al.'s work.[14] In this work, gaskets were made of gold-plated Ni-base Alloy 718. Because the optical surface of the sapphire was degraded by pitting corrosion in high temperature water during the study, a 0.25 mm thick CVD diamond disk was placed on the water side of the sapphire window and this has greatly reduced surface attack on the sapphire window. The Alloy 600 specimen was held in the recess of an oxidized zirconium metal by an Alloy 718 washer with the gasket of an oxidized zirconium sheet in order to electrically insulate the specimen for the cell.

The Raman spectroscopy system is consisted of an excitation laser source, a spectrometer and optical components including mirrors and filters. Fig. 2 shows the layout drawing of optical system with near backscattering geometry including optical cell and water chemistry loop used in this work. A more detailed description for the developed Raman system is given elsewhere.[15]

The chemical condition of typical PWR primary water was used. Water with a resistivity of 18 MΩ-cm was mixed with chemicals to produce 1,000 ppm boron in the form of boric acid (H_3BO_3) and 2 ppm lithium in the form of lithium hydroxide (LiOH). Two different levels of hydrogen concentration were prepared with corresponding dissolved hydrogen concentrations of 2.68 ppm and 0.089 ppm (30 cm^3(STP)/kg or 1 cm^3(STP)/kg) at 25℃, respectively, according to the solubility data.[13] The operating pressure was about 18 MPa and the temperature was increased from room temperature to 350℃. Measurements were after stabilizing temperature at 250, 290, 320 and 350 C, respectively. At the conclusion of experiment the cell was cooled and a specimen was analyzed by the Raman system in room temperature air.

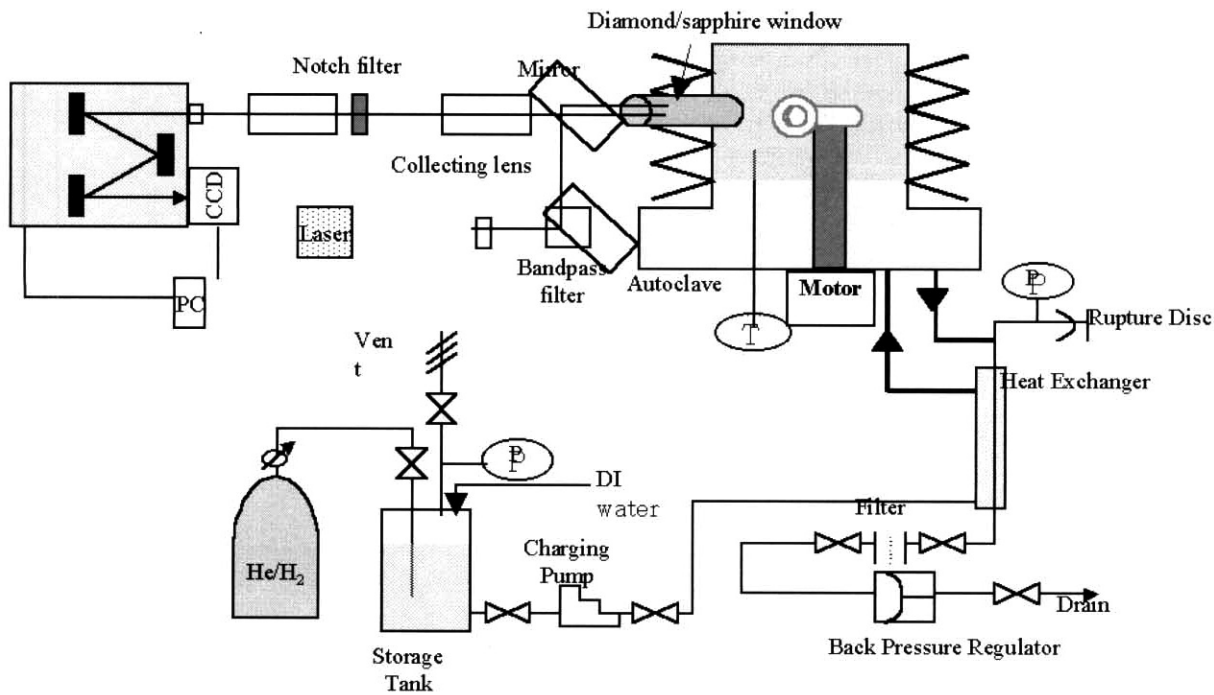

Fig. 2. Layout of in-situ Raman spectroscopic measurement system in high temperature aqueous environment.

2.3 Morphology of oxide film on Alloy 600

Upon the completion of in-situ Raman spectroscopic measurements, the Alloy 600 specimen was removed from the cell for microstructural examinations. Fig. 3 shows the morphology of the surface oxide film observed by a field emission scanning electron microscope (FE-SEM) after series of exposures that ended at 350°C PWR water for 110 hours. The surface oxide film is composed of a compact layer by small crystallites of few tens of nm in diameter. Scattered crystallites of about 200 nm in diameter are present on the compact layer.

Fig. 4 shows the transmission electron micrographs on a cross-section of Alloy 600 specimen oxidized in simulated PWR water with 30 cm^3(STP)/kg of dissolved hydrogen concentration for 71 hours. The thickness of oxide film on Alloy 600 was observed to be in the range of 12~180 nm. Compact layers and other crystalline phases on Alloy 600 observed by TEM have the same morphology as those in the FE-SEM micrographs of Fig. 3.

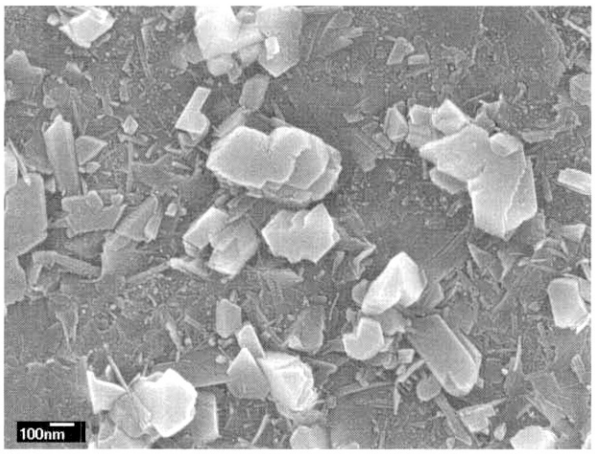

Fig. 3. Field emission scanning electron micrographs of oxide film on Alloy 600 after 110 hours exposure in simulated PWR water.

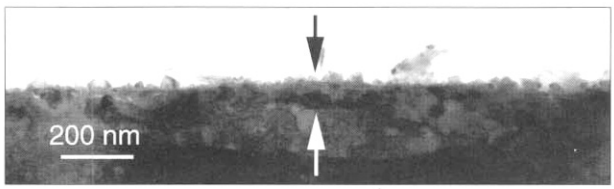

Fig. 4. TEM micrographs of oxide film on Alloy 600 after 71 hours exposure in simulated PWR water.

3. Results

3.1 Reference raman spectra for high purity oxide powders

The first series of experiments were conducted to obtain reference Raman spectra on pure oxides using powder samples. Results were compared with literature data in order to verify the developed system. The results of experiments with nickel and chromium oxides and spinels in room temperature air environment are summarized in Table 2. As shown in Table 2, the Raman features of the reference spectra for high purity powders show good agreements between the measurement in this work and literature data.[16)-19)] Further details of results in this study are given elsewhere.[15)]

Table 2. Nominal Raman Peak Wavenumbers for Oxide Powders[a] Measured in Room Temperature Air Environment.

Oxide	This work[b]	Ref. A[c]	Ref. B[c]
NiO	1,074	1,074 [16)]	
	910	913 [16)]	
	725	727 [16)]	
	532	535 [16)]	490 [16)]
	400	370 [16)]	
$NiFe_2O_4$	702	705 [17)]	700 [18)]
	654^{sh}	655 [17)]	655 [18)]
	595	592 [17)]	
	574	570 [17)]	579 [18)]
	492	488 [17)]	490 [18)]
	460	457 [17)]	433 [18)]
Cr_2O_3	610	613 [19)]	585 [19)]
	550	552 [19)]	554 [19)]
	528	527 [19)]	488 [19)]
	352	350 [19)]	387 [19)]
	302	300 [19)]	352 [19)]
$NiCr_2O_4$	687	685 [17)]	686 [18)]
		616 [17)]	
		585 [17)]	
	550-560	554 [17)]	
	513	514 [17)]	512 [18)]
	429	430 [17)]	

[a] The most intense peak(s) in each spectrum is underlined.
[b] The wavenumber of a well-resolved peak has an associated uncertainty of ± 2 cm^{-1}.
[c] The excitation laser with 647.1 nm wavelength was used.

3.2 In-situ raman observation in PWR water with 30 cm^3(STP)/kg of dissolved hydrogen concentration

To maintain the dissolved hydrogen concentration (DH_2) of 30 cm^3(STP)/kg in the simulated PWR water, pure hydrogen gas was injected into the water storage tank with the cover gas pressure of 170 kPa. Based on Henry's law, a dissolved hydrogen concentration of 2.68 ppm is expected.[13] The operating pressure was about 18 MPa and the temperature was gradually increased from room temperature to 350℃ at an average rate of 40℃/hour. Temperatures at which Raman spectra were collected with the remained time length are summarized in Table 3.

Fig. 5 shows the in-situ Raman spectra of Alloy 600 specimen obtained by holding temperatures at 250, 290, 320, and 350℃, respectively, while temperature increased. Peaks observed at ca. 417 cm^{-1}, 743 cm^{-1} in the in-situ Raman spectra were originated from the sapphire window. A feature in the range of ca. 546-587 cm^{-1} in the spectrum acquired at 250℃ was known to be attributed to α-CrOOH based on Maslar et al.'s work.[19] According to the explanation described in Ref. 19, [$Cr^{III}O_6$] octahedral are common structure to both Cr_2O_3 and (-CrOOH.[21] Therefore, one might reasonably expect the Raman wave numbers of α-CrOOH to be observed in approximately the same wave number range as those of Cr_2O_3, i.e., ca. 300-613 cm^{-1}.

Table 3. Temperature and Exposure Time of Alloy 600 Specimen Prior to In-Situ Raman Spectra Measurements in High Temperature Water.

DH_2 (cc/kg)	Temperature (℃)	Total exposure time prior to first measurement at temperature (h)	Hold time at each temperature prior to first measurement (h)
30	250	28	2
	290	33.5	3
	320	42	7
	350-I	47.5	3.5
	350-II	69.5	20.5
1	250	40	33
	290	45	3
	320	48	2
	350-I	51	2
	350-II	74	23

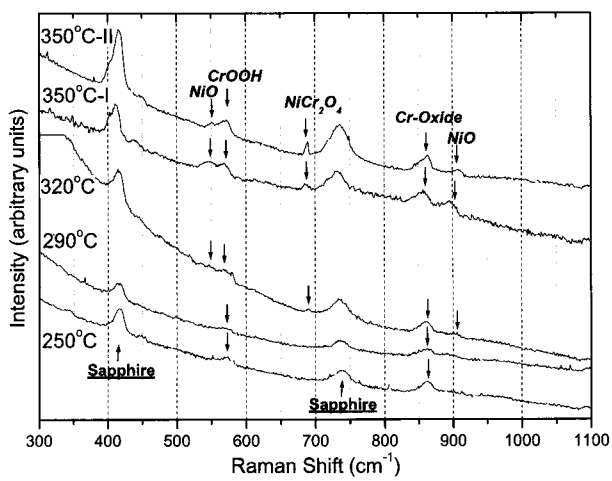

Fig. 5. In-situ Raman spectra obtained for Alloy 600 by holding at 250, 290, 320 and 350℃, respectively, during heating up to 350 ℃ in PWR water condition with DH_2=30cc(STP)/kg.

The crystallographic structure of the $Cr_2O_3 \cdot nH_2O$ powder is yet unknown. The $Cr_2O_3 \cdot nH_2O$ XRD pattern does not match any chromium hydrate/hydroxide reference patterns.[19] The broad XRD peaks are typical of a hydrate consisting of a mixture of different metastable hydrates/hydroxides. This result is consistent with a report on the $Cr_2O_3 \cdot nH_2O$ possessing variable water content.[22] While the observed Raman peaks for $Cr_2O_3 \cdot nH_2O$ cannot be attributed to a particular structural characteristic, the $Cr_2O_3 \cdot nH_2O$ Raman spectrum illustrates that the Raman peaks of some hydrated Cr^{III} oxide are observed in approximately the same wave number range as those of Cr_2O_3. Additionally, the infrared (IR) spectrum of α-CrOOH exhibits features in this wave number range, i.e., peaks at 525 and 610 cm^{-1}.[23] Therefore, the shared structural features of Cr_2O_3 and α-CrOOH and the wave number range of the Raman features in the Cr_2O_3 and $Cr_2O_3 \cdot nH_2O$ reference spectra are consistent with the assignment of the measured Raman features to α-CrOOH.

Several intense peaks are also observed in the 840-880 cm^{-1} range of spectra in Fig. 5. According to the extensive discussion by Maslar et al.[19], this feature would be attributed to Cr^{VI} or crystalline Cr^{III}/Cr^{VI} species assuming a chromium species is responsible for this feature. This explanation can account for the weak signature observed in the 340-350 cm^{-1} range in the spectra of the specimen at 250℃. Chromium oxide features in this wave number range are generally attributed to Cr^{VI}-oxygen terminal stretching modes or mixed Cr^{III}/Cr^{VI} oxide vibrational modes.[24] Hydrated surface chromate species have been reported to exhibit a vibrational mode at ca. 865 cm^{-1}.[25] The most intense peak in the aqueous $HCrO_4^-$ Raman spectrum was reported from ca. 880 to 899 cm^{-1}.[26),27] A number of mixed Cr^{III}/Cr^{VI} oxides have been identified during the thermal decomposition of various chromium-containing materials. Crystalline chromium oxide compounds such as Cr_3O_8, Cr_2O_5, and XCr_3O_8 (X = Na, K, Rb) exhibit their most intense Raman spectral features in

the ca. 820-904 cm^{-1} range at room temperature. The most intense Raman spectral feature of an amorphous Cr^{III}/Cr^{VI} compound has been observed at 859 cm^{-1}. In the spectra obtained at 250 ℃ and 290 ℃, weak features appeared at 704 cm^{-1} that were attributed to nickel ferrite spinel ($NiFe_2O_4$) features.

In the spectra obtained at 320 ℃, features of pure chromium oxide including α-CrOOH, Cr^{VI} and crystalline Cr^{III}/Cr^{VI} compounds become weaker, while nickel oxide features are firstly observed and become more apparent in subsequent spectra up to 350℃. The features at 550 cm^{-1} and 910 cm^{-1} were attributed to NiO phase. Also, features of nickel chromium spinel ($NiCr_2O_4$) were detected in this temperature range. The features at ca. 682 cm^{-1} and 430 cm^{-1} were attributed to $NiCr_2O_4$ phase.[17),18)] Also, nickel oxide and nickel chromite phase were still detected on the specimen surface as exposure time increases at 350℃. The $NiCr_2O_4$ is one of thermodynamically stable phases in a reducing aqueous environment with the range of hydrogen overpressure at about 300℃. A more detail study that was performed to identify thermodynamically stable phase of nickel base alloy in high temperature water was described in ref. 28.

3.3 In-situ Raman observation in PWR water with 1 cm^3(STP)/kg of dissolved hydrogen concentration

To maintain the dissolved hydrogen concentration of 1 cm^3(STP)/kg in water, 5% hydrogen gas balanced with 95% helium gas was injected into the water with the overpressure of 0.7 atm and it made a dissolved hydrogen concentration of 0.089 ppm in this study.[13)] Temperatures at which Raman spectra were collected with the remained time length are summarized in Table 3.

Fig. 6 shows the in-situ Raman spectra of Alloy 600 specimen obtained at the lower hydrogen concentration while temperature increased. A feature in ca. 546-587 cm^{-1} range in the spectrum acquired at 250℃ was attributed to α-CrOOH from the same rationale as that described earlier in the result with DH_2 = 30 cc/kg. Also, the intense peaks feature that would be attributed to Cr^{VI} or crystalline Cr^{III}/Cr^{VI} species was observed in the 840-880 cm^{-1} range.

As temperature increased, clear features in 550 and 910 cm^{-1} which were attributed to nickel oxide (NiO) were firstly appeared and became weaker in subsequent spectra up to 350℃. After 23 hours at 350℃ in this condition, the features of nickel oxide phase were still detected on the Alloy 600 specimen surface at 350℃.

3.4 Effect of dissolved hydrogen concentration change in PWR water

To investigate the effect of dissolved hydrogen con

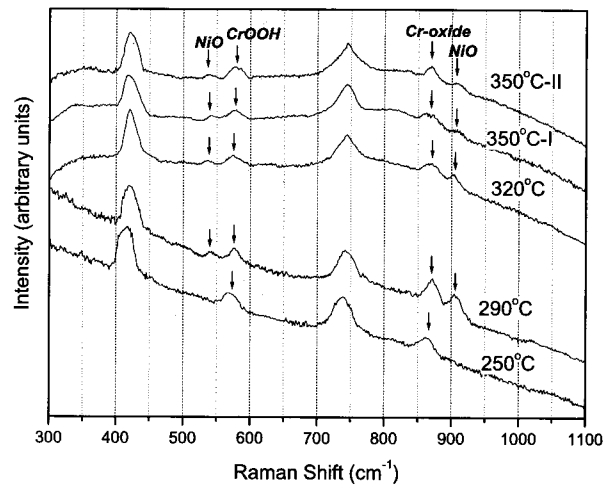

Fig. 6. In-situ Raman spectra obtained for Alloy 600 by holding at 250, 290, 320 and 350℃, respectively, during heating up to 350℃ in PWR water condition with DH_2=1cc(STP)/kg.

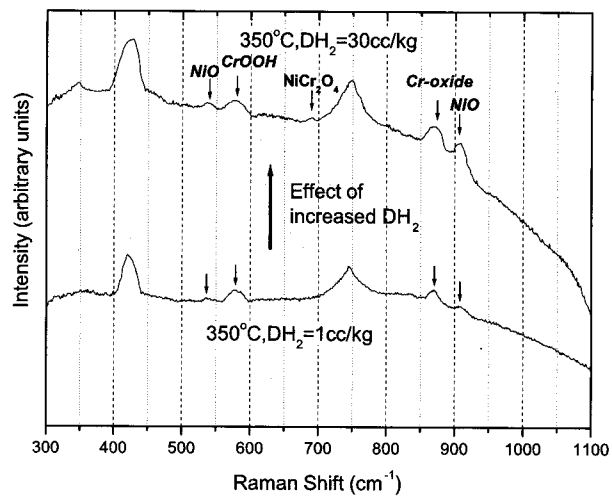

Fig. 7. In-situ Raman spectra obtained for Alloy 600 at 350℃ in PWR water as the DH_2 in water was increased from 1 to 30 cc/kg.

centration on the formation of oxide film of Alloy 600 in high temperature water, dissolved hydrogen concentration was increased from 1 to 30 cc/kg, immediately following the measurement at 1 cc/kg. In-situ Raman spectroscopic measurement of Alloy 600 surfaces was made both before and after the change of hydrogen concentration.

Fig. 7 shows the change of Raman spectra with the increase of dissolved hydrogen concentration in water at 350℃. In high temperature water with 1 cc/kg of hydrogen concentration, features of pure chromium oxide including α-CrOOH, Cr^{VI} and crystalline Cr^{III}/Cr^{VI} compounds and

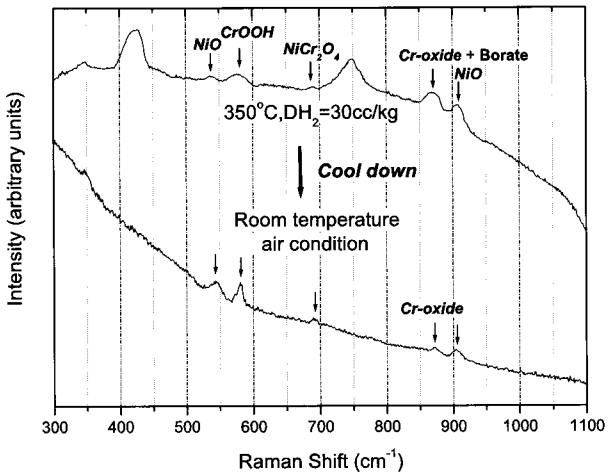

Fig. 8. Comparison of Raman spectra obtained for Alloy 600 between by in-situ method at 350℃ in PWR water with DH_2 =30 cc/kg and by ex-situ method in room temperature and air condition.

nickel oxide (NiO) features were observed at the oxide film of Alloy 600 specimen. With the increase of dissolved hydrogen concentration, nickel chromium spinel ($NiCr_2O_4$) features were appeared in the observed Raman spectrum.

3.5 Comparison between in-situ and ex-situ Raman spectra

Fig. 8 represents the ex-situ Raman spectrum for the surface film on Alloy 600 specimen obtain in room temperature air after it was cooled down from high temperature observations. Results are compared with the in-situ Raman spectrum oxide film of Alloy 600 in 350℃ water with $DH_2 = 30$ cc/kg. As shown in Fig. 8, it can be seen that only the intensity of a peak at ca. 870 cm^{-1} in the ex-situ spectra was weakened comparing with that in the in-situ spectra.

According to earlier work by Gui and Devine[29] and Melendres et al.[30], the feature appeared at ca. 870 cm^{-1} was known to be attributed to the total symmetric stretch vibration of borate ions located in the water. Also, the feature appeared at this range of wave number was known to be originated from chromium oxides, as previously explained at the part of in-situ experimental results in this study, following the extensive discussion in Maslar et al.'s work.[19] Consequently, it can be concluded that Cr-oxide peak and borate peak coincided with each other at ~870 cm^{-1} and the intensity of the Raman peak at ca. 870 cm^{-1} in the ex-situ spectra was weakened by the absence of borate ion.

4. Discussion

4.1 Observation vs. prediction of oxide film composition

Table 4 summarizes the experimental observations of surface oxide phases of Alloy 600 in 350℃ water in comparison with literature data[10),12),31)] at each dissolved hydrogen concentration. At higher dissolved concentration, $NiFe_2O_4$ precipitates reported in ref. 10 and 31 could be made by Fe ion dissolution from high temperature flowing system including autoclave, tubes and fitting for longer exposure time than this work. Also, from the viewpoint of diffusion kinetics, the difference between results of this study and of previous studies could be considered to be caused by differences between diffusion coefficients of alloying elements. However, the affected oxide thickness by kinetic decomposition is very small compared to the whole oxide thickness. Assuming the Fe ion diffusivity in nickel oxide of 10^{-19} cm^2/sec at 350 degree C and the average thickness of a whole oxide of alloy 600 in this study of 100 nm, the diffusion distance of Fe ion from the substrate alloy across oxide film is approximately 1 nm per one day (24 hours). It is very small amount of

Table 4. Summary of Experimental Observations of Surface Oxide Phases Of Alloy 600 in 350℃ Water in Comparison with Literature Data at Each Dissolved Hydrogen Concentration.

	This work	Soustelle[10)]	Caron[12)]	Nakagawa[31)]
Method	In-situ Raman	GDOS + EDS	XPS	Synchrotron XRD + TEM
Temperature (℃)	350	360	330	320
Exposure time (hrs)	70	300	1869	1000
Oxide(s) at high DH_2	CrOOH Cr-Oxide $NiO+NiCr_2O_4$	Compact layer ($NiCr_2O_4$)+ Precipitates ($NiFe_2O_4$)	$NiCr_2O_4$	(Ni+Cr-rich) oxide + Precipitates ($NiFe_2O_4$)
Oxide(s) at low DH_2	CrOOH Cr-Oxide NiO	Compact layer ($NiCr_2O_4$)	NiO	NiO

distance in comparison with a whole oxide thickness. Therefore it can be said that the effect of kinetic decomposition is negligible for the condition employed in this work. As the oxide growth rate is expected to decrease with time, a more detail investigation of kinetic phase change of oxide needs to be performed for long-term oxidation experiments. At lower dissolved concentration, the hydroxide phase of CrOOH undetected by previous ex-situ methods, was observed under most conditions in this study and it shows a useful aspect of the in-situ method since the removal of the material from the corrosion environment can result in modification of the oxide film structure and chemistry. The observed NiO phase at lower dissolved concentration agrees well with those reported in literature.

From the viewpoint that electrochemical potential-pH diagrams can be useful in predicting thermodynamically stable phases, thermochemical calculations can provide very much meaningful information to explain the corrosion behavior of Alloy 600 in high temperature water. Although the pH was not measured at high temperature and pressure during this investigation, this value can be estimated using aqueous thermochemical calculation softwares. In this work, pH values of primary water in PWR were calculated as a function of temperature using MULTEQ®.[32] Electrochemical potential value was calculated by using the Nernst equation assuming that the surface of Alloy 600 behaves as a hydrogen electrode in the hydrogen-containing water environment. The potential of hydrogen electrode is given as below;

$$E_{H^+/H_2}(T) = E^{\circ}_{H^+/H_2}(T) - 2.303\frac{RT}{2F}\left[\log f_{H_2} + 2pH\right]$$
$$= -2.303\frac{RT}{2F}\left[\log f_{H_2} + 2pH\right] \quad vs.\,SHE(T)$$

Table 5 summarizes the comparison between experimental observations and thermochemical prediction of oxide phases of Alloy 600 at each condition of temperature and hydrogen concentration. It can be known that the consideration of formation of chromium oxide hydroxide (CrOOH) and nickel spinels can make differences in the thermochemical prediction results, regardless of dissolved hydrogen concentration in 350℃ water. At both conditions of dissolved hydrogen concentration, nickel ferrite ($NiFe_2O_4$) phases that were predicted to be thermodynamically stable assuming that nickel spinels can be formed in this system were not experimentally detected. When the observed oxide phases are compared with the predicted stable phases of Alloy 600 at 350℃, all the observed oxide phases but Cr-oxides are included in predicted stable phases. But the thermochemical predictions with CrOOH and Ni spinels do not agree with the observed results at both hydrogen concentrations in 350℃ water. In contrast, the predicted Ni/NiO equilibrium line is in good agreement with the observed results. This suggests that relatively simple oxide phases identified by in-situ Raman spectroscopic investigation can be used to verify thermodynamically stable phases.

Table 5. Summary of in-situ Raman Observations and Thermochemical Predictions of Surface Oxide Phases of Alloy 600 in 350℃ Water with the Assumption of Different Oxides.

	Predicted at 350 ℃			Observed at 350 ℃
		With Ni spinels	Without Ni spinels	
DH_2 = 30cc/kg	With CrOOH	CrOOH $NiFe_2O_4$	CrOOH NiO	NiO $NiCr_2O_4$ CrOOH Cr-Oxide
	Without CrOOH	$NiCr_2O_4$ $FeCr_2O_4$	NiO $FeCr_2O_4$	
DH_2 = 1cc/kg	With CrOOH	CrOOH $NiFe_2O_4$	CrOOH NiO	NiO CrOOH Cr-Oxide
	Without CrOOH	$NiCr_2O_4$ $FeCr_2O_4$	NiO $FeCr_2O_4$	

In-situ Raman spectroscopy is shown to be a very useful experimental tool that can provide valuable information about oxide films and the SCC behavior of Alloy 600 in high temperature aqueous environments. In this work, dissolved hydrogen concentration was experimentally known to play an important role on the formation of oxide films on the Alloy 600 in high temperature water. Different compositions of oxides were produced at different conditions of dissolved hydrogen concentration in high temperature water.

4.2 Ni/NiO thermodynamic equilibrium

From the results of in-situ Raman spectra measurements of Alloy 600 with the increase of temperature, dissolved hydrogen concentration is one of the most important experimental parameters in this study. While nickel oxide was observed at 320℃ or higher at the higher hydrogen concentration, nickel oxide was observed at 290℃ or higher at the lower hydrogen concentration. To compare experimental results with calculations, thermochemical calculations for Alloy 600 were made as a function of temperature, as described in ref. 28. In this calculation, for simplicity, it was assumed that nickel oxide could be produced whereas spinel oxide could not form. Fig. 9 summarizes both the experimental results of in-situ Raman observation with two different levels of dissolved hydrogen concentration and the thermochemical calculation

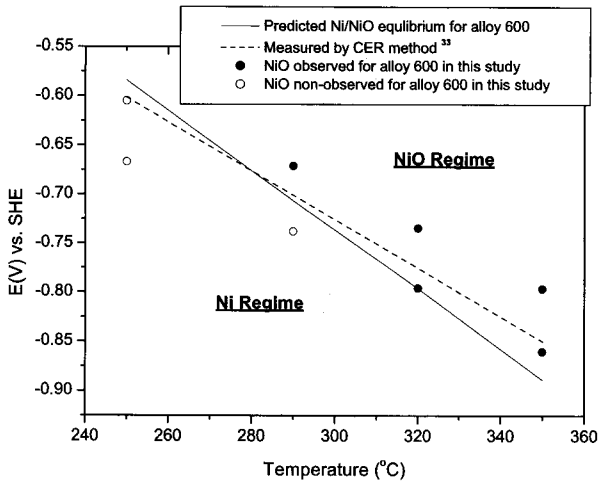

Fig. 9. Summary plot on electrochemical potential for nickel in the Alloy 600 as a function of temperature.

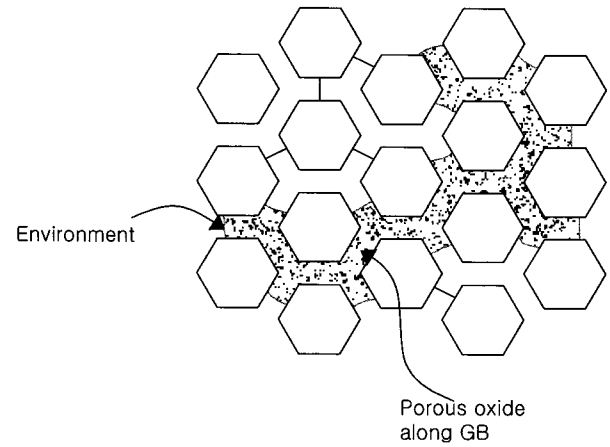

Fig. 10. Postulated Redox-induced GB Oxide Degradation Mechanism.

of Ni/NiO equilibrium as a function of temperature. In Fig. 9, dashed line represents a previous experimental result of nickel/nickel oxide transition using a contact electric resistance (CER) instrument by Attanasio et al.[33] By comparison between this and previous results, it can be seen that a good agreement was found between in-situ Raman results and those from contact electrical resistance (CER) measurements on Ni/NiO equilibrium.

4.3 Implication to PWSCC mechanism

Previous studies[10),11)] showed that there exists a critical dissolved hydrogen concentration at high temperature corresponding the maximum susceptibility of Alloy 600 to PWSCC. The present in-situ Raman spectroscopic study showed that the phase changes between nickel metal (Ni) and nickel oxide (NiO) and the thermodynamic equilibrium of Ni/NiO were clearly observed over relatively narrow range of dissolved hydrogen concentration in high temperature water. Under experimental conditions in the vicinity of Ni/NiO, it is likely ECP can fluctuate due to uncontrollable variations in temperature, hydrogen concentration, and water pH. Similar variation can be expected during actual PWR operations. Therefore it is conceivable that electrochemical condition of PWR water can cross Ni/NiO equilibrium repeatedly.

It was previously reported that oxide phase change from one to another can cause stress-induced degradation of oxide integrity and hence is responsible for an accelerated corrosion in zirconium alloys[34)] and Cu[35)] in nuclear power plants. Recently, it was clearly demonstrated that the PWSCC sensitivity of Alloy 600 was increased in high temperature water with dissolved hydrogen concentration corresponding to Ni/NiO equilibrium condition.[36)] Considering large difference in their molar volumes, alteration of water chemistry cross Ni/NiO can severely undermine oxide integrity due to high stresses involved.

From the observed PWSCC behavior, it can be postulated that repeated phase changes between Ni metal and NiO occurs more rapidly along grain boundaries due to faster diffusion. Consequently, degradation of oxide integrity can enhance the percolation of oxidant preferentially along grain boundaries to accelerate PWSCC. The redox-induced grain boundary oxide degradation mechanism is depicted in Fig. 10. To verify this postulation, a series of PWSCC testing can be performed with cycling of dissolved hydrogen concentration from lower (higher) DH_2 via DH_2 corresponding to Ni/NiO equilibrium to higher (lower) DH_2 in high temperature water. From the mitigation standpoint based on redox-induced oxide degradation and percolation, it may be suggested that the dissolved hydrogen concentration in water should be controlled more precisely and/or should be maintained at relatively lower contents far away from Ni/NiO equilibrium condition in order to reduce PWSCC sensitivity of Alloy 600 in nuclear power plants.

5. Conclusions

In-situ Raman spectroscopic investigation has been conducted for surface oxide films on a nickel-base Alloy 600 exposed to simulated PWR primary water with 1,000 ppm boron and 2 ppm lithium at a pressure of 18 MPa, for temperatures ranging up to 350°C and dissolved hydrogen concentrations ranging from 1 to 30 cc/kg in an optically accessible high-pressure cell. From this study, following conclusions are made:

1. An in-situ Raman spectroscopic system was developed successfully to provide valuable information for the

oxide film in PWR water conditions.

2. At the lower dissolved hydrogen concentration (1 cm^3(STP)/kg), nickel oxide(NiO) phase was detected on the specimen surface at temperature ranges between 290 and 350℃. Nickel oxide phase appeared to be stable over a long period of time (21 hours) at 350 ℃.

3. At the higher dissolved hydrogen concentration (30 cm^3(STP)/kg), chromium oxide hydroxide (CrOOH) phase was detected on the specimen surface at relatively low temperature ranging from 250℃ to 290℃. Also, features attributed to the phase of NiO and $NiCr_2O_4$ were observed at 320℃ or higher.

4. Some unique observations were made, compared with earlier ex-situ results;

① CrOOH phase, undetected by ex-situ methods, was observed under most conditions.

② $NiFe_2O_4$ usually found in precipitate layer was not observed, conceivably due to the suppression of precipitate layers in this work.

5. NiO, Cr_2O_3 and $NiCr_2O_4$ phases were observed, in reasonable agreement with ex-situ results.

6. Ni/NiO equilibrium was determined as function of dissolved hydrogen concentration and temperature.

① Comparison of observed results with thermodynamic predictions showed a good agreement on Ni/NiO equilibrium at the temperature range from 250 to 350 degree C.

② A good agreement was found between in-situ Raman results and those from contact electrical resistance (CER) measurements on Ni/NiO equilibrium.

7. From the result of this study, a new postulation that redox alteration between Ni metal and NiO can enhance oxide degradation presumably along grain boundaries and facilitate the percolation of oxidants to accelerate. A test of the postulation is planned using the in-situ Raman system.

Acknowledgements

The authors would like to express their gratitude to Dr. J. Maslar and Dr. W. Hurst of the National Institute of Standards and Technology, Gaithersburg, MD, USA. Professor Y.W. Kim of Seoul National University kindly helped electron microscope examinations. This work was supported by the Post-doctoral Fellowship Program of Korea Science & Engineering Foundation(KOSEF). Also, this study was Supported by Korea Institute of Science & Technology Evaluation and Planning(KISTEP) and Ministry of Science & Technology(MOST), Korean government, through its National Nuclear Technology Program.

References

1. J.M. Gras, "Stress corrosion cracking of steam generator tubing materials - review and assessment", Parkins Symposium on Fundamentals Aspects of Stress Corrosion Cracking, TMS, 1992, p.411.
2. T.M. Angeliu, P.L. Andresen, and F.P. Ford, "Applying slip-oxidation to the SCC of austenitic materials in BWR/PWR environments", Corrosion 98, NACE (1998), Paper No.262.
3. T. Magnin, J-M. Boursier, D. Noel, R. Rios, and F. Vaillant, "Corrosion-deformation interaction during stress corrosion cracking of alloy 600 in primary water", Proceedings of the 6th International Symposium on Environmental Degradation of Materials in Nuclear Power System - Water Reactors, TMS, 1993, p.669.
4. P.M. Scott and M. Le Calvar, "Some possible mechanisms of intergranular stress corrosion cracking of alloy 600 in primary water", Proceedings of the 6th International Symposium on Environmental Degradation of Materials in Nuclear Power System - Water Reactors, TMS, 1993, p.657.
5. P.M. Scott, "An Overview of internal oxidation as a possible explanation of intergranular stress corrosion cracking of alloy 600 in PWRs", Proceedings of the 9th International Symposium on Environmental Degradation of Materials in Nuclear Power System - Water Reactors, TMS, 1999, p.3.
6. G. Was, T.M. Angeliu, and J.K. Sung, "Deformation and intergranular cracking behavior of Ni-Cr-Fe alloys at high temperature", Proceedings of the "Specialist Meeting on Environmental Degradation of Alloy600", Airlie House, VA, April 1993, EPRI Report TR-104898, 1996, p.24-1.
7. M.M. Hall, "Thermally activated low temperature creep and primary water stress corrosion cracking of NiCrFe alloys", Proceedings of the "Specialist Meeting on Environmental Degradation of Alloy600", Airlie House, VA, April 1993, EPRI Report TR-104898, 1996, p.6-1.
8. R.S. Pathania, and A.R. McIlree, "A review of the effect of hydrogen on stress corrosion cracking of alloy 600 in 360℃ water", Proceedings of the 3rd International Symposium on Environmental Degradation of Materials in Nuclear Power System - Water Reactors, AIME, 1987, p.551.
9. T. Cassagne and A. Gelpi, "Crack growth rate measurements an alloy 600 steam generator tubing in primary and hydrogenated AVT water", Proceedings of the 8th International Symposium on Environmental Degradation of Materials in Nuclear Power System - Water Reactors, TMS, 1993, p.679.
10. C. Soustelle, M. Foucault, and P. Combrade, "PWSCC of alloy 600: a parametric study of surface film effects", Proceedings of the 9th International Symposium on Environmental Degradation of Materials in Nuclear Power System - Water Reactors, TMS, 1999, p.105.
11. T. Cassagne, B. Fleury, F. Vaillant, O. De Bouvier, and P. Combrade, "An Update of the Influence of

Hydrogen on the PWSCC of nickel base alloy in high temperature water", Proceedings of the 8th International Symposium on Environmental Degradation of Materials in Nuclear Power System - Water Reactors, TMS, **1**, 307 (1997).
12. D. Caron, PhD. Thesis, INSA-Lyon Scientific and Technical University, France, 2000.
13. D.M. Himmelblau, "Solubilities of inert gases in water 0℃ to near the critical point of water", *J. Chem. Eng. Data*, **5**, 10 (1960).
14. W.S. Hurst, M.S. Hodes, W.J. Bowers Jr., V.E. Bean, J.E. Maslar, and K.A. Smith, "Optical flow cell and apparatus for solubility, salt deposition and Raman spectroscopic studies in aqueous solutions near the water critical point", Journal of Supercritical Fluids 22 (2002): p.151.
15. J.H. Kim and I.S. Hwang, "Development of in-situ Raman spectroscopic system of surface oxide films of metals and alloys in high temperature water conditions", *submitted to Nuclear Engineering and Design (Feb., 2004)*.
16. J.E. Maslar, W.S. Hurst, W.J. Bowers Jr., J.H. Hendricks, and M.I. Aquino, "In situ Raman spectroscopic investigation of nickel hydrothermal corrosion", Corrosion **58**, 225 (2002).
17. J.E. Maslar, W.S. Hurst, W.J. Bowers Jr., and J.H. Hendricks, "In situ Raman spectroscopic investigation of stainless steel hydrothermal corrosion", Corrosion **58**, 739 (2002).
18. M.D. Cunha Belo, "Composition, structure and properties of the oxide films formed on the stainless steels 316L in a primary type PWR environment", *Corrosion Science*, **40**, 447 (1998).
19. J.E. Maslar, W.S. Hurst, W.J. Bowers Jr., J.H. Hendricks, M.I. Aquino, and I. Levin, "In situ Raman spectroscopic investigation of chromium surface under hydrothermal conditions", *Applied Surface Science*, **180**, 102 (2001).
20. R.L. McCreery, Raman spectroscopy for chemical analysis, (Wiley-Interscience, 2000).
21. A.F. Well, Structural inorganic chemistry, 5th ed., (Oxford: Clarendon Press, 1984).
22. F.A. Cotton, and G. Wilkinson, Advanced inorganic chemistry, A comprehensive test, 5th ed. (New York, NY:Wiley, 1980).
23. R.G. Snyder and J.A. Ibers, "O-H-O and O-D-O potential energy curves for chromous acid", *J. Chem. Phys.* **36**, 1356 (1962).
24. J.E. Maslar, W.S Hurst, T.A. Vanderah, and I. Levin, "The Raman spectra of Cr_3O_8 and Cr_2O_5", *J. Raman Spectrosc.* **32**, 201 (2001).
25. B.M. Weckhuysen, I.E. Wachs, and R.A. Schoonheydt, "Surface chemistry and spectroscopy of chromium in inorganic oxides", *Chem. Rev.* **96**, 3327 (1996).
26. J.B.B. Heyns, J.J. Cruywagen, and K.T. Carron, "Raman spectroscopic investigation of chromium (VI) equilibrium-another look", *J. Raman Spectrosc.* **30**, 335 (1999).
27. G. Michel and R. Machiroux, "Raman spectroscopic investigation of the $Cr_2O_4^{2-}/Cr_2O_{47}^{2-}$ equilibrium in aqueous solution", *J. Raman Spectrosc.* **14**, 22 (1983).
28. J.H. Kim, Ph. D. Dissertation, Seoul National University, Republic of Korea (2003)
29. J. Gui and T. M. Devine, "The influence of sulfate ions on the surface enhanced raman spectra of passive films formed on iron", *Corros. Sci.* **36**, 441 (1994).
30. C. A. Melendres, J. Acho and R. L. Knight, *J. Electrochem. Soc.* **138**, 877 (1991).
31. T. Nakagawa, N. Totsuka, T. Terachi, and N. Nakajima, "Influence of dissolved hydrogen on oxide film and PWSCC of alloy 600 in PWR primary water," *Journal of Nuclear Science and Technology*, **40**, 39 (2003).
32. "MULTEQ, Equilibrium of an electrolytic solution with vapor-liquid partitioning, Volume 3: Theory manual", EPRI NP-5561-CCML, Vol. 3, EPRI, Palo Alto, CA, 1992.
33. S.A. Attanasio, D.S. Morton, M.A. Ando, N.F. Panayotou, and C.D. Thompson, "Measurement of the nickel/nickel oxide phase transition in high temperature hydrogenated water using the contact electric resistance (CER) techniques", Proceedings of the 10th International Symposium on Environmental Degradation of Materials in Nuclear Power System - Water Reactors, NACE, 2001.
34. E. Hillner, Zirconium in the Nuclear Industry, ASTM STP 633, p.211, Philadelphia, 1977.
35. B.G. Park, I.S. Hwang, "Corrosion induced clogging and plugging in water-cooled generator cooling circuit", International conference on water chemistry in nuclear reactors systems, Chimie 2002, Avignon, France, April 22-26, 2002.
36. D.S. Morton, S.A. Attanasio, and G.A. Young, "Primary water SCC understanding and characterization through fundamental testing in the vicinity of the nickel/nickel oxide phase transition", Proceedings of the 10th International Symposium on Environmental Degradation of Materials in Nuclear Power System - Water Reactors, NACE, 2001.